

# GREEN BANK TELESCOPE OBSERVATIONS OF THE WATER MASERS OF NGC 3079: ACCRETION DISK MAGNETIC FIELD AND MASER SCINTILLATION

W. H. T. VLEMMINGS<sup>1</sup>, H. E. BIGNALL<sup>2</sup> & P. J. DIAMOND<sup>1</sup>  
*For the Astrophysical Journal*

## ABSTRACT

We present observations of the 22 GHz H<sub>2</sub>O megamasers in the circumnuclear disk of NGC 3079 obtained with the Green Bank Telescope. The data are analyzed for circular polarization due to the Zeeman-induced splitting of the H<sub>2</sub>O maser lines. No circular polarization is detected and we derive a 1 $\sigma$  upper limit of 11 mG for the toroidal magnetic field at  $\sim 0.64$  pc from the central black hole. This is the tightest upper limit for the magnetic field around a black hole to date. We use the magnetic field limit to derive an estimate of the mass accretion onto the central black hole. In addition to the polarimetric results, we present an observation of rapid variability in the maser lines, which we explain as weak interstellar scintillation. From the scintillation parameters, we estimate an intrinsic size of the mostly saturated maser features of  $\sim 12$  microarcseconds. This is consistent with models assuming a thick, clumpy accretion disk.

*Subject headings:* galaxies: individual (NGC 3079)—magnetic fields—masers—scattering

## 1. INTRODUCTION

Since AGN are thought to be powered by accretion onto a central super-massive black hole in which magnetic fields likely play an important role (e.g. Blandford & Payne 1982), substantial magnetic fields are expected to be present throughout the entire accretion disk. Observations of H<sub>2</sub>O maser circular polarization induced by Zeeman-splitting are an extremely useful method of probing the magnetic field in regions where H<sub>2</sub>O masers occur. Weak Zeeman splitting was initially observed in interstellar H<sub>2</sub>O masers using the Effelsberg 100 m telescope by Fiebig & Güsten (1989) and has since been used to determine the strength and structure of magnetic fields in star-forming regions (e.g. Sarma et al. 2002; Vlemmings et al. 2006) and in the envelopes of late-type stars (e.g. Vlemmings et al. 2002).

Recently, Herrnstein et al. (1998) and Modjaz et al. (2005) (hereafter M05) have used both the Very Large Array (VLA) and Green Bank Telescope (GBT) in an attempt to measure the circular polarization of the H<sub>2</sub>O megamasers in the circumnuclear disk of NGC 4258. The recent observations of M05 have placed stringent upper limits on the circumnuclear magnetic field of NGC4258. Here we present GBT observations of the H<sub>2</sub>O masers in the circumnuclear disk of NGC 3079 that were aimed at measuring the H<sub>2</sub>O maser Zeeman splitting due to the magnetic field in the disk.

NGC 3079 is an almost edge-on spiral galaxy at approximately 16 Mpc (Sofue 1999). It shows either Seyfert-2 or LINER activity and there is strong evidence from X-ray data that it contains an active galactic nucleus (AGN) (e.g. Irwin & Saikia 2003; Kondratko et al. 2005, and references therein). NGC 3079 also contains one of the most luminous 22 GHz H<sub>2</sub>O megamasers known to date (e.g. Henkel et al. 1984). Like that in NGC 4258, the H<sub>2</sub>O maser emission of NGC 3079 has been interpreted as originating in a circumnuclear disk (e.g. Trotter et al. 1998; Sawada-Satoh et al. 2000; Yamauchi et al. 2004; Kondratko et

al. 2005) , although the exact disk models proposed differ between authors. Kondratko et al. (2005) (hereafter K05) recently produced the first map of the full extent of the 22 GHz H<sub>2</sub>O maser emission of NGC 3079 (between  $V_{\text{LSR}} \approx 880 \text{ km s}^{-1}$  and  $1400 \text{ km s}^{-1}$ ) and propose a model in which the accretion disk of NGC 3079 is thick, clumpy, flaring and undergoing star-formation. NGC 3079 is also the site of the first detected extragalactic submillimeter H<sub>2</sub>O masers, which also originate from the nuclear region (Humphreys et al. 2005).

In addition to the measurement of Zeeman splitting, the GBT observations have allowed us to study the short-term variability of the masers. Previously, line flux variability of several tens of per cent on timescales of minutes has been observed for 22 GHz H<sub>2</sub>O megamasers of the Circinus galaxy (Greenhill et al. 1997; McCallum et al. 2005). As the timescale of intrinsic maser variations are at least an order of magnitude larger, the Circinus maser variability is likely due to a combination of weak and diffractive interstellar scintillation (McCallum et al. 2005). Here we present the first measurements of short timescale variability of the NGC 3079 H<sub>2</sub>O megamasers and discuss the variability in the context of interstellar scintillation.

## 2. OBSERVATIONS & DATA REDUCTION

The observations of the H<sub>2</sub>O megamasers in NGC 3079 were carried out at the NRAO<sup>3</sup> GBT between April 10 and April 19 2006. At 22.2 GHz the full-width at half maximum (FWHM) beamwidth of the GBT is  $\sim 33''$ , several orders of magnitude larger than the size of the H<sub>2</sub>O maser region, which is contained within approximately 30 mas. The GBT spectrometer was used with a bandwidth of 200 MHz and 16,384 spectral channels. This resulted in a channel spacing of  $0.164 \text{ km s}^{-1}$  and a total velocity coverage of  $2700 \text{ km s}^{-1}$  , which was centered on  $V_{\text{LSR}} = 1116 \text{ km s}^{-1}$ . Furthermore, the data were taken with the dual-polarization receiver of the lower *K*-band (frequency range: 18.0–22.5 GHz) using the total power nod observing mode. The two beams have a

<sup>3</sup> The National Radio Astronomy Observatory (NRAO) is a facility of the National Science Foundation operated under cooperative agreement by Associated Universities, Inc.

<sup>1</sup> Jodrell Bank Observatory, University of Manchester, Macclesfield, Cheshire SK11 9DL, U.K.; wouter@jb.man.ac.uk

<sup>2</sup> Joint Institute for VLBI in Europe, Postbus 2, 7990 AA Dwingeloo, Netherlands

fixed separation of  $178.8''$  in the azimuth direction and a cycle time of 2 minutes was sufficient to correct for atmospheric variations. As a result, one beam of the telescope was always pointing at the source while the other beam was used for baseline correction. The total observing time was 30.2 hours of which 20.9 hours were spent on source. Once every  $\sim 1.2$  hr point and focus observations were done on J0958+655. This source was also used as flux calibrator. The pointing corrections resulted in a pointing accuracy typically better than  $\sim 2''$ . System temperatures ranged between 35 and 55 K, although an observing block of  $\sim 5$  hr suffered from bad weather and as a result had a higher system temperature of  $\sim 65$  K.

For data reduction the GBT IDL<sup>4</sup> software package was used. The observations of J0958+655 yielded a gain-curve over the entire observation session which was linearly interpolated between calibrator observations and applied to the NGC 3079 data. Over the full observation run, the gain does not change by more than 10%, while the variation over several hours in the flux density of J0958+655 is  $< 5\%$ . Assuming that J0958+655 is not circularly polarized and that the circular polarization of the continuum emission of NGC 3079 is negligible, both the calibrator and the source data were used to determine a constant gain offset between the RCP and LCP data. It was found that the RCP gain needed to be multiplied by a factor 0.945 to produce a Stokes  $V$  ( $= (RCP - LCP)/2$ ) spectrum without signal. To remove residual baseline variations due to atmospheric and instrumental effects as well as removing the continuum emission from NGC 3079, we subtracted a baseline determined using the spectral channels free of maser emission. We estimate the absolute flux calibration to be accurate to  $\sim 10\%$ . As the magnetic field determination depends on the S/N and not the absolute flux levels, this uncertainty does not influence the field strength determination. Finally, we produce source spectra in Stokes I and V, seen in Fig. 1, as well as RCP and LCP for the total combined data set. We find, from the spectral channels without signal, that we reach a  $1\sigma$  noise level of 1.4 mJy for I and V, while for RCP and LCP the noise level is 2.1 mJy. As the GBT observations presented here constitute hitherto the most sensitive observations of the H<sub>2</sub>O megamasers of NGC 3079, Fig. 2 shows a rescaled, hanning smoothed, total power spectrum highlighting the faint maser emission. The  $1\sigma$  noise level in this hanning smoothed spectrum is 0.9 mJy.

### 3. RESULTS & DISCUSSION

#### 3.1. Maser Saturation

Theoretical analysis in Nedoluha & Watson (e.g 1992) has shown that the degree of circular polarization of the 22 GHz H<sub>2</sub>O masers depends on the level of maser saturation. The 22 GHz H<sub>2</sub>O masers begin to saturate when  $R/\Gamma \gtrsim 1$  s<sup>-1</sup> and approach full saturation when  $R/\Gamma \gtrsim 100$  s<sup>-1</sup>, where  $R$  is the rate of stimulated emission and  $\Gamma$  is the maser decay rate. Following the analysis in M05, we find for the stimulated emission rate of the H<sub>2</sub>O masers of NGC 3079 at 16 Mpc

$$R = 250 \left( \frac{S_\nu}{1 \text{ Jy}} \right) \left( \frac{L}{10^{16} \text{ cm}} \right)^{-2} \text{ s}^{-1}. \quad (1)$$

<sup>4</sup> <http://gbtdl.sourceforge.net>

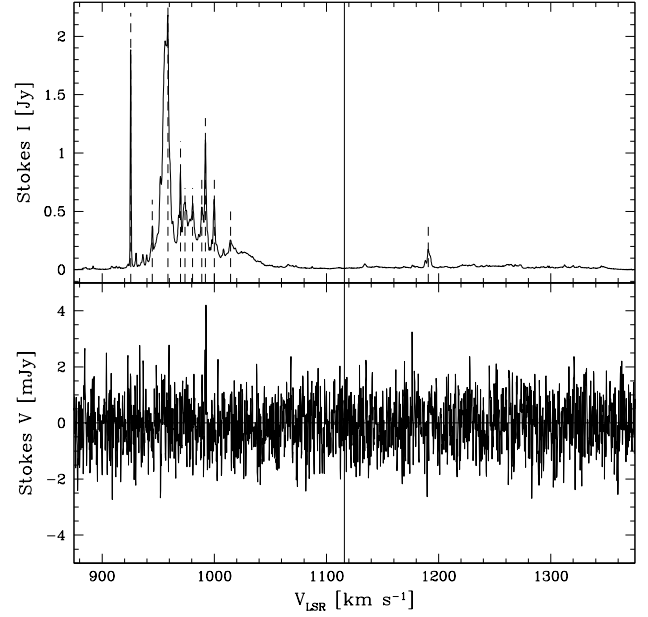


FIG. 1.— Average total intensity (I, top) and circular polarization (V, bottom) spectrum of the NGC 3079 H<sub>2</sub>O megamasers. The solid vertical line at  $v_{\text{LSR}} = 1116 \text{ km s}^{-1}$  indicates the systemic velocity. The dashed vertical lines indicate the maser features for which the variability parameters are given in Table 2.

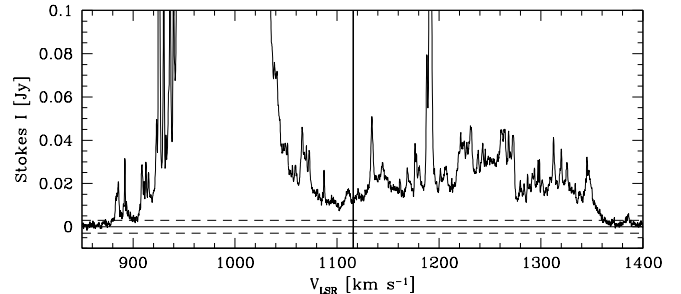


FIG. 2.— Rescaled hanning smoothed total intensity spectrum of the NGC 3079 H<sub>2</sub>O megamasers highlighting the faintest detected maser flux. The solid vertical line indicates the systemic velocity. The dashed horizontal lines give the  $3\sigma$  rms level of the hanning smoothed spectrum.

Here we assume a cylindrical maser model with  $L$  the maser length and  $S_\nu$  the maser flux density. The clumpy maser disk model from K05 predicts clump sizes between 0.001 and 0.006 pc. Taking these sizes as limits on the maser length  $L$ , we find  $70(S_\nu/1 \text{ Jy}) < R < 2600(S_\nu/1 \text{ Jy}) \text{ s}^{-1}$ . The lifetime of the IR transitions involved in the maser process  $\Gamma = 1 \text{ s}^{-1}$ , and the typical maser features are between 0.25 and 0.5 Jy; we thus conclude that most of the H<sub>2</sub>O masers of NGC 3079 are at least partially saturated and that several of the masers are even fully saturated. This is in contrast to the mostly unsaturated masers of NGC 4258 (M05) and to the prediction of  $R/\Gamma \lesssim 1$  from numerical simulations by Watson & Wyld (2000). It is worth noting that the models from Watson & Wyld (2000) are specifically tailored for the thin accretion disk of NGC 4258 and are thus unlikely to be applicable

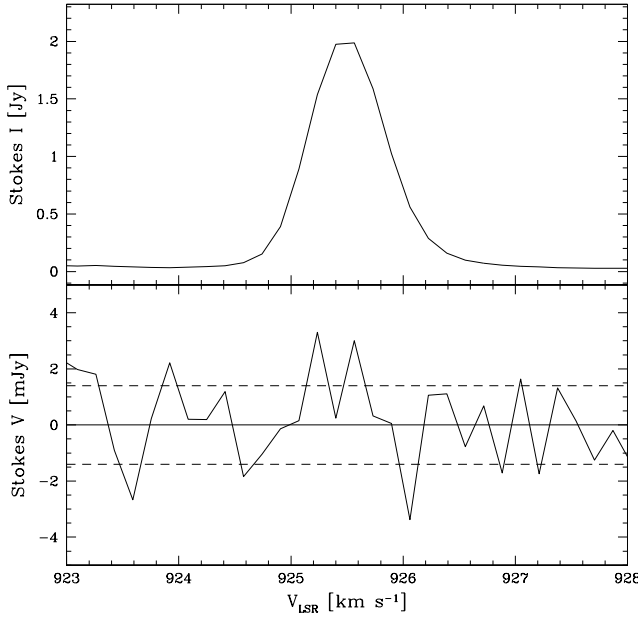


FIG. 3.— Average total intensity ( $I$ , top) and circular polarization ( $V$ , bottom) spectrum of the  $925.5 \text{ km s}^{-1}$  blue-shifted  $\text{H}_2\text{O}$  maser feature of NGC 3079. The dashed horizontal lines in the  $V$ -spectrum indicate the  $\pm 1\sigma$  errors.

to the thick, clumpy accretion disk of NGC 3079. For high saturation, the spectral FWHM linewidth is expected to be  $\Delta v \approx 1.3 \text{ km s}^{-1}$  (e.g. Nedoluha & Watson 1992; Vlemmings et al. 2002) for masering gas at intrinsic temperatures  $T \sim 300 \text{ K}$ . In Table 2, we notice that although the majority of the maser lines reach the expected width, several of the strongest lines have a  $\Delta v \sim 0.9 \text{ km s}^{-1}$ . This either indicates that these lines are only partly saturated, that the intrinsic thermal line width of these lines is smaller, or a combination of these effects, thus highlighting various different conditions throughout the maser disk.

### 3.2. The Magnetic Field

As the  $\text{H}_2\text{O}$  maser lines in the spectrum of NGC 3079 are very blended, we used the RCP-LCP cross-correlation method described in M05 to determine the Zeeman splitting and corresponding magnetic field strength for both the red- and blue-shifted masers. This cross-correlation method is specifically suited for blended maser lines of non-paramagnetic maser species, assuming the magnetic field is mostly constant across the spectrum, and it has been used to determine the upper limit of the magnetic field strength from the 22 GHz  $\text{H}_2\text{O}$  maser polarization spectra of NGC 4258. As described in M05, the cross-correlation method yields the velocity shift  $q$  due to the Zeeman effect, which is directly related to the magnetic field strength along the line of sight  $B_{||}$  by

$$B_{||} = \frac{q}{\sqrt{2}A_{F-F'}}. \quad (2)$$

Here  $A_{F-F'}$  is the coefficient that describes the relation between the circular polarization and the magnetic field for a transition between a high ( $F$ ) and low ( $F'$ ) rotational energy level. The coefficient depends both on the intrinsic maser thermal width and the maser saturation

level (Nedoluha & Watson 1992; Vlemmings et al. 2002). Here we have used  $A_{F-F'} = 0.020 \text{ km s}^{-1} \text{ G}^{-1}$ , as derived by Nedoluha & Watson (1992) for the merging of the three dominant 22 GHz  $\text{H}_2\text{O}$  maser hyperfine transitions. The results of this analysis are given in Table 1, where the rms error in velocity shift  $q$ , determined as described in the appendix of M05, yields the error in  $B_{||}$ . As the red-shifted masers are weak, the  $1\sigma$  error on the  $B_{||}$ -field determination is large, and as no significant magnetic field detection is made, we determine the  $3\sigma$  upper limit to be 807 mG. The error on the magnetic field in the blue-shifted masers is significantly smaller, but still no significant Zeeman splitting was detected. Here the  $3\sigma$  upper limit is 33 mG, hitherto the tightest upper limit on the magnetic field in an accretion disk.

In addition to the cross-correlation method for the heavily blended maser spectrum, an isolated  $\text{H}_2\text{O}$  maser line at  $V_{\text{LSR}} = 925.5 \text{ km s}^{-1}$  also allows us to derive the magnetic field using the regular Zeeman method (Vlemmings et al. 2002). Here the magnetic field is determined using

$$P_V = \frac{(V_{\text{max}} - V_{\text{min}})}{I_{\text{max}}} = 2A_{F-F'}B_{||}/\Delta v, \quad (3)$$

where the fractional circular polarization  $P_V$  is determined from the maximum and minimum circular polarization  $V_{\text{max}}$  and  $V_{\text{min}}$  and the peak total intensity  $I_{\text{max}}$ . The coefficient  $A_{F-F'}$  is described above and is again taken to be  $0.020 \text{ km s}^{-1} \text{ G}^{-1}$ , and  $\Delta v$  is the maser FWHM. As seen in Fig. 3, no significant detection is made in the circular polarization spectrum. Using the calculation of the rms error limit as described in Vlemmings et al. (2006), we find a  $3\sigma$  upper limit of  $B_{||} = 48 \text{ mG}$ , similar to the upper limit determined on the blue-shifted masers with the cross-correlation method.

Assuming a standard accretion disk model, the magnetic field measurements at the blue and red-shifted maser features probe the toroidal magnetic field  $B_{\phi}$  at an average distance to the central black hole of  $\sim 0.64 \text{ pc}$ . Since we found that the masers appear to be either partially or fully saturated, the measured magnetic field strength could overestimate the true field strength by up to a factor of 4 (Vlemmings et al. 2002, fig. 7). However, velocity gradients along the maser path can cause the true magnetic field strength to be underestimated by up to a factor of two (Vlemmings 2006). Additionally, the blending of maser lines in single-dish measurements can also lead to further underestimation of the actual field strength by a factor of two (Sarma et al. 2001). As we determined a similar upper limit on the isolated maser line at  $V_{\text{LSR}} = 925.5 \text{ km s}^{-1}$  as on the blended blue-shifted masers, we adopt the conservative  $3\sigma$  upper limit of  $B_{\phi} = 33 \text{ mG}$  for the actual toroidal magnetic field strength. Using the model predictions for the magnetic field configuration in an accretion disk from Hawley et al. (1996) as described in M05,  $B_{\phi}$  dominates the total magnetic field and  $B_{\text{tot}} \approx (16/10)^{1/2}B_{\phi}$ . We thus take the total magnetic field strength to be  $B_{\text{tot}} \lesssim 40 \text{ mG}$  at a radius of  $0.64 \text{ pc}$ . Such a field strength value falls in the lower range of the magnetic field strengths observed for the  $\text{H}_2\text{O}$  masers in Galactic starforming regions (e.g. Fiebig & Güsten 1989; Sarma et al. 2002; Vlemmings et al. 2006). Comparing to the limits found for NGC 4258 while taking into account the difference in the limit calculations, the magnetic field limit of NGC 3079 found in this paper

TABLE 1  
MAGNETIC FIELD UPPER LIMITS

Maser line(s)	Fitted velocity interval (km s <sup>-1</sup> )	$\Delta_v$ (km s <sup>-1</sup> )	$I_0$ (Jy)	$B_{  }$ (mG)	$\sigma_{B_{  }}$ (mG)	$ B_{  }^{\text{lim}} $ (mG)
925.503 km s <sup>-1</sup> feature	923.5–927.5	1.913	0.81	-	16	48
Red-shifted lines	1175–1375	-	-	349	269	807
Blue-shifted lines	900–1100	-	-	-9	11	33

is  $\sim 2.5$  times lower at 0.64 pc than that at 0.14 pc in NGC 4258.

### 3.2.1. Mass Accretion Rate

The mass accretion rate in the disk of NGC 3079 can be estimated from the magnetic field strength using the relation between the thermal pressure and the magnetic pressure within the accretion disk. Adapting formula 7 from M05 to the case of NGC 3079 gives for the mass accretion rate  $\dot{M}$

$$\dot{M} \lesssim 10^{-1.5} \frac{0.6\beta}{1+\beta} \left( \frac{B_{\text{tot}}}{40 \text{ mG}} \right)^2 \left( \frac{T_k}{400 \text{ K}} \right)^{1/2} \times \left( \frac{r}{0.64 \text{ pc}} \right)^3 \left( \frac{M_{\text{BH}}}{2 \times 10^6 M_{\odot}} \right)^{-1} M_{\odot} \text{yr}^{-1} \quad (4)$$

Here  $T_k$  is the temperature of the maser gas,  $r$  the distance to the central black hole and  $M_{\text{BH}}$  the black hole mass. The ratio between gas and magnetic pressure  $\beta$  is estimated from local three-dimensional MHD calculations to be  $\langle \beta \rangle \approx 60$  (Hawley et al. 1996).

Thus for our total magnetic field upper limit of  $B_{\text{tot}} = 40 \text{ mG}$  we find  $\dot{M} \lesssim 10^{-1.7} M_{\odot} \text{yr}^{-1}$  at  $r = 0.64 \text{ pc}$ , assuming a smooth magnetic field configuration. As this estimate is based on the average magnetic field strength across the maser region, a much more complex magnetic field structure would lead to a higher upper limit by at most an order of magnitude. We can compare this upper limit to the estimate of the mass accretion rate found in K05 for their model of a thick, clumpy accretion disk. They find an accretion rate of  $0.007 L_{\text{bol,10}} M_{\odot} \text{yr}^{-1}$ , where  $L_{\text{bol,10}}$  is the AGN bolometric luminosity in units of  $10^{10} L_{\odot}$ . With an estimate of the AGN bolometric luminosity from X-ray data of  $\sim 5 \times 10^9$ – $5 \times 10^{10} L_{\odot}$  this indicates  $10^{-2.5} < \dot{M} < 10^{-1.5} M_{\odot} \text{yr}^{-1}$ . Thus our result for the mass accretion rate is fully consistent with the K05 model and implies an AGN bolometric luminosity of  $\lesssim 2.9 \times 10^{10} L_{\odot}$ , which in turn implies an Eddington ratio of  $\lesssim 0.4$ .

### 3.3. Variability

Although the peak flux has varied by up to 50%, the overall shape of the total intensity spectrum in Fig. 1 is strikingly similar to the earlier spectrum from 2003 seen in figure 3 of K05. The only major difference is the appearance of a strong, somewhat isolated blue-shifted feature at  $V_{\text{lsr}} = 925.5 \text{ km s}^{-1}$ . As shown in Fig. 4, this feature, in contrast with the other maser features, shows a steady decline in flux. Our time baseline is not sufficient to determine a non-linear flux decrease. Using an error weighted, least squares fit to our individual observing scans of 4 minutes yields a decrease in flux of 64 mJy/day. There are several possible mechanisms that can explain such gradual,

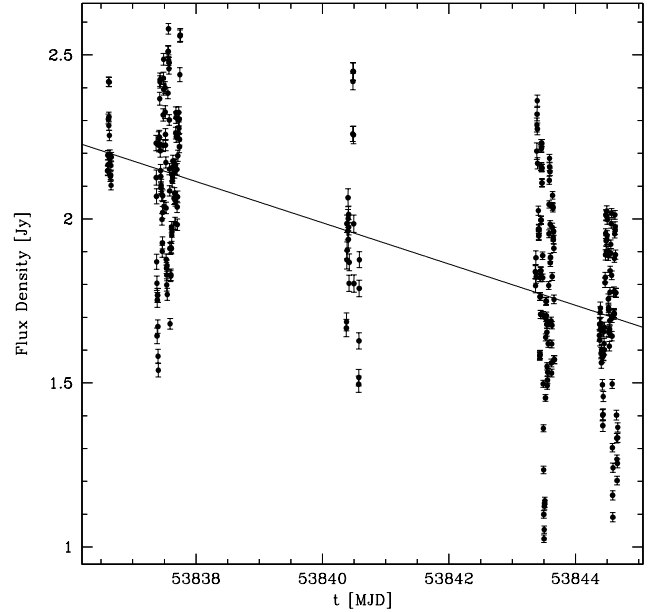


FIG. 4.— The light curve of the 925.503 km s<sup>-1</sup> blue-shifted H<sub>2</sub>O maser feature over the entire observation run. The thick solid line is a weighted least square fit to a simple linear decrease in flux density and corresponds to a decrease of 64 mJy per day.

time-variable behavior (Maloney 2002). One possibility is a time-variable maser pump. The H<sub>2</sub>O megamasers could be powered by X-ray emission from the AGN, as discussed by Neufeld et al. (1994). Variations in the AGN would then result in variations in the H<sub>2</sub>O maser flux. However, although the location of the  $V_{\text{LSR}} = 925.5 \text{ km s}^{-1}$  with respect to the other maser features is unknown, one would expect correlated flux variation in at least some of the other maser lines. Another more likely explanation is, that the variability is caused by the amplification of background emission from another maser feature. As the disk of NGC 3079 is thought to be strongly inhomogeneous, the maser emission is narrowly beamed along the line-of-sight by the overlap of maser regions with similar Doppler velocities. As discussed in K05, chance alignments of maser regions will then result in variability at timescales of several days or longer.

### 3.4. Scintillation

In addition to the longterm variability seen in the feature at  $V_{\text{LSR}} = 925.5 \text{ km s}^{-1}$ , the maser features of NGC 3079 also vary on timescales of several tens of min-

TABLE 2  
VARIABILITY PARAMETERS OF THE NGC 3079 H<sub>2</sub>O MASERS LINES

Velocity (km s <sup>-1</sup> )	$\Delta v$ (km s <sup>-1</sup> )	$\langle S \rangle$ (Jy)	$\sigma_S$ (Jy)	$\mu$	$T_{\text{char}}$ (hr)	Depth of First Minimum
925.503 ± 0.003 <sup>a</sup>	0.81 ± 0.01	1.913	0.255	0.133	0.26 ± 0.03	-0.41 ± 0.08
944.92 ± 0.02	0.77 ± 0.09	0.378	0.042	0.110	0.34 ± 0.04	-0.30 ± 0.09
958.660 ± 0.006	0.89 ± 0.02	2.195	0.197	0.090	0.27 ± 0.04	-0.03 ± 0.06
969.84 ± 0.01	1.05 ± 0.03	0.847	0.089	0.105	0.27 ± 0.05	-0.32 ± 0.10
973.53 ± 0.04 <sup>b</sup>	3.4 ± 0.2	0.584	0.050	0.086	0.40 ± 0.10	-0.13 ± 0.09
980.89 ± 0.03	1.45 ± 0.14	0.576	0.047	0.081	0.44 ± 0.07	-0.21 ± 0.09
988.93 ± 0.04 <sup>b</sup>	1.4 ± 0.2	0.539	0.045	0.090	0.31 ± 0.05	-0.13 ± 0.09
992.16 ± 0.01	1.30 ± 0.06	1.122	0.097	0.087	0.34 ± 0.03	0.09 ± 0.07
999.89 ± 0.01	1.34 ± 0.06	0.612	0.083	0.136	0.35 ± 0.03	-0.28 ± 0.08
1014.45 ± 0.04 <sup>b</sup>	3.3 ± 0.2	0.256	0.025	0.096	0.38 ± 0.10	-0.08 ± 0.15
1190.65 ± 0.03	1.48 ± 0.05	0.177	0.025	0.139	0.37 ± 0.05	-0.27 ± 0.18

<sup>a</sup>For the variability analysis the linear flux decrease has been removed.

<sup>b</sup>Heavily blended feature.

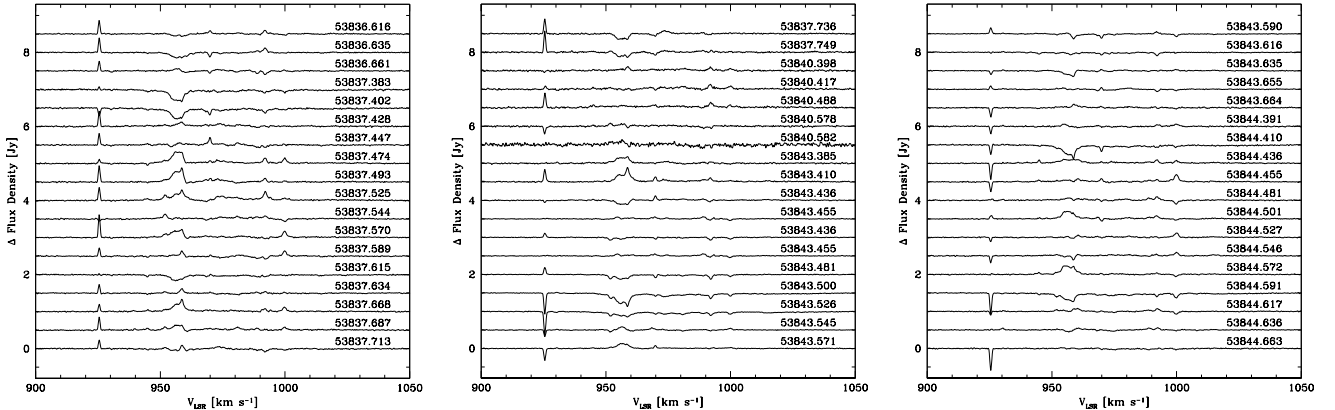


FIG. 5.— The variability of the blue-shifted H<sub>2</sub>O masers of NGC 3079. The spectra are averaged over 24 minutes, corresponding to 6 observing scans. The average total intensity I spectrum from Fig. 1 has been subtracted for each of the spectra which are labeled with the MJD of the observation. Each spectrum is off-set by 0.5 Jy and the rms noise in the spectra is  $\sim 3.4$  mJy.

utes as seen in Fig. 5. Such rapid variability has been previously observed for the H<sub>2</sub>O megamasers of Circinus (Greenhill et al. 1997; McCallum et al. 2005). As seen in Fig. 6, in which 7 hours of observation on the strongest red- and blue-shifted masers are shown, the observed variations reach the level of 50% within the hour. This is similar to the flux variation seen in Circinus. Although small variations in time due to incorrect antenna gain corrections might still be present, the hour to hour gain variations determined from the observations of J0958+55 are not expected to be  $> 5\%$ . However, as the gain corrections using J0958+55 are only performed every 1.2 hours after correcting the telescope pointing, accumulated pointing uncertainties and elevation effects can cause a global gain variation of up to  $\approx 10\text{--}25\%$  between two consecutive observing blocks. While such large variations only occur 6 times during our total observation run, the most extreme of these instances can be seen during the first hour of observations presented in Fig. 6. These occasions are found to have no significant effect on our determination of the

variability characteristics. An additional indication that the observed variability is not due to calibration errors is the fact that we find no significant correlation in the variability of the different maser lines.

To characterize the variability we have determined the discrete autocorrelation function (Dacf) following Edelson & Krolik (1988). The Dacf of one of the maser lines is shown in Fig. 7. Following Rickett et al. (2002), we define the characteristic timescale for variability,  $T_{\text{char}}$ , as the time-lag where the Dacf falls to 0.5. We further determine the depth of the first Dacf minimum and the modulation index  $\mu = \sigma / \langle S \rangle$ . Here  $\langle S \rangle$  is the mean peak flux of the maser line and  $\sigma$  the rms of the variability. The variability parameters are given in Table 2 along with the local standard of rest (LSR) velocity,  $V_{\text{LSR}}$ , and the full-width half-maximum ( $\Delta v$ ). The velocity and  $\Delta v$  are determined from fitting Gaussian profiles to the maser spectrum. However, many of the maser features are heavily blended, increasing the uncertainties in the velocity and  $\Delta v$  determinations. We find that  $T_{\text{char}}$  ranges from  $\sim 900$

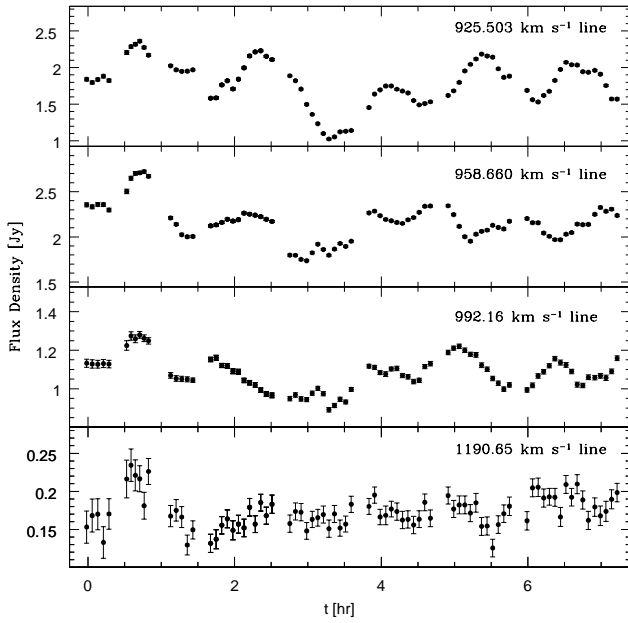


FIG. 6.— Light curves of the three strongest blue-shifted  $\text{H}_2\text{O}$  maser lines of NGC 3079 as well as that of the strongest red-shifted line (bottom) observed on April 17th and 18th 2006. Data points are plotted for every 4 minute observing scan. In the top two panels, the error bars are smaller than the symbol size. The typical  $1\sigma$  error bar is  $\sim 18$  mJy. The light curve of the maser feature at  $925.503 \text{ km s}^{-1}$  has been corrected for the linear flux decrease shown in Fig. 4.

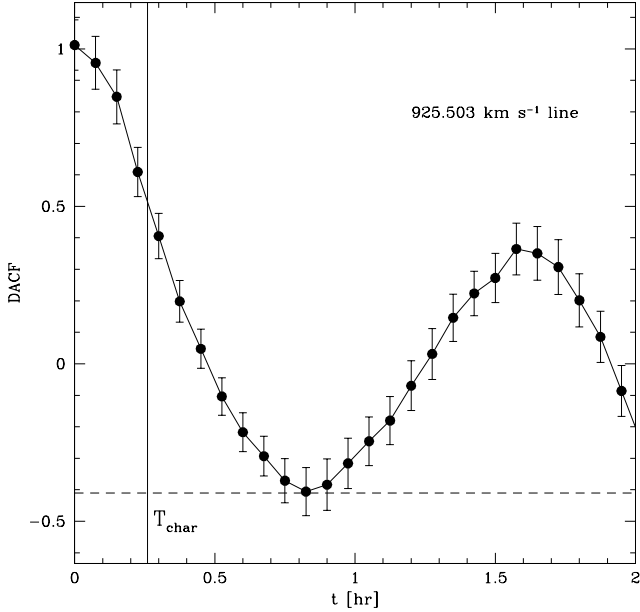


FIG. 7.— Discrete, normalized autocorrelation function (Dacf) of the  $925.503 \text{ km s}^{-1}$  maser line. The lags are binned in 4.5 min intervals. The Dacf and the  $1\sigma$  error bars are calculated following Edelson & Krolik (1988). The solid vertical line indicates the characteristic variability timescale  $T_{\text{char}}$ , where  $\text{Dacf} = 0.5$  and the dashed horizontal line is the first negative.

to  $\sim 1600$  s.

As shown in McCallum et al. (2005), the variability of

$\sim 700$  s of the Circinus  $\text{H}_2\text{O}$  masers is likely due to a combination of weak and diffractive scintillation. However, NGC 3079 is located at much higher galactic latitude ( $b = +48.36^\circ$ ) than Circinus, for which the line of sight passes through the galactic plane. From the Galactic electron density model NE2001 (Cordes & Lazio 2002), we find at the position of NGC 3079 that the predicted transition frequency between weak and strong scintillation is  $\nu_0 = 8.8$  GHz. The model uncertainties of NE2001 are significant at high latitude and for individual lines-of-sight, however NGC 3079 can reasonably be expected to be in the weak scintillation regime at 22.2 GHz.

Using formula 6 from Walker (1998) for the frequency dependence of modulation index for a point source in the weak scintillation regime, we find from our observations, with a typical modulation index  $\mu = 0.1$ , the implied transition frequency between weak and strong scintillation is  $\nu_0 = 4.4$  GHz. The transition frequency would be higher if the maser size invalidates the point source approximation. If the angular source size  $\theta_S$  is larger than the angular size of the first Fresnel zone  $\theta_F$  at the distance of the scattering screen, then the modulation index is decreased. At 22.2 GHz,  $\theta_F = 59(z/1\text{pc})^{-1/2} \mu\text{as}$ , where  $z$  is the distance of the scattering screen. Assuming saturation, cylindrical masers are beamed by a factor of  $\sim 3$  (Elitzur 1994). As the clump sizes in the maser disk are estimated in K05 to be between 0.001 and 0.006 pc, this yields for the beamed masers, at 16 Mpc, an angular size between 4 and 25  $\mu\text{as}$ . As several maser features are only partly saturated, the beaming is more pronounced, and the angular sizes are even smaller. Thus, taking a typical maser size of  $\theta_S = 10 \mu\text{as}$ , the scattering screen would need to be at  $z \sim 150$  pc to satisfy  $\theta_S/\theta_F \approx 2.3$  if the transition frequency is in fact close to the NE2001 model  $\nu_0 = 8.8$  GHz. It is interesting to note that our calibration source J0958+655 (B0954+658), at an angular separation of  $9.9^\circ$  from NGC 3079, showed the prototypical extreme scattering event in 1980-81 (Fiedler et al. 1987), which was suggested by Fiedler et al. (1994) as being possibly associated with the edge of Galactic Loop III at a distance of 145 pc.

However, a distant screen implies a long scintillation timescale. At 22.2 GHz, the variability timescale for a point source is  $t_F = 8100 V_{\text{ISM}}^{-1} z^{1/2}$ , with  $V_{\text{ISM}}$  being the transverse speed of the scattering screen with respect to the source in  $\text{km s}^{-1}$ . For  $\theta_S > \theta_F$ , the characteristic variability timescale  $T_{\text{char}} = t_F(\theta_S/\theta_F)$ . Thus for a screen at  $z = 150$  pc and  $\theta_S/\theta_F = 2.3$ ,  $T_{\text{char}} = 2.3 \cdot 10^5 V_{\text{ISM}}^{-1} \text{ s}^{-1}$ . To reconcile this with the typical observed timescale of 1200 s requires  $V_{\text{ISM}} \approx 190 \text{ km s}^{-1}$ , which is much larger than the expected value of  $V_{\text{ISM}} \approx 40 \text{ km s}^{-1}$  corresponding to the velocity of the Earth with respect to the LSR in the direction of NGC 3079 at the date of the observation.

Alternatively, the observed rapid variations and lower transition frequency compared to the NE2001 model prediction could result from scattering in a nearby screen, as has been found for the handful of extremely rapid “intra-hour” scintillating quasars (Dennett-Thorpe & de Bruyn 2000; Rickett et al. 2002; Bignall et al. 2003). Although there are some exceptions, the maser lines in Table 2 have a tendency to display the smallest  $T_{\text{char}}$  and largest  $\mu$  for those lines with the lowest  $\Delta v$ , which are thus thought to

be only partially saturated. This would be consistent with the corresponding maser features being the smallest due to the increased maser beaming. We thus expect  $\theta_S \lesssim \theta_F$  for the partially saturated sources and expect  $\theta_S$  to be slightly larger than  $\theta_F$  for the fully saturated sources. Taking  $T_{\text{char}} \approx 1000$  s from partially saturated masers to be  $t_F$ , we find that the velocity and the screen distance have to satisfy  $z^{1/2} = 0.12 V_{\text{ISM}}$ . For  $V_{\text{ISM}} \approx 40 \text{ km s}^{-1}$  for a screen moving with the local standard of rest, this indicates  $z \approx 25 \text{ pc}$ . This in turn gives  $\theta_S \approx \theta_F = 12 \mu\text{as}$ , thus the maser feature sizes expected from the scintillation are consistent with those estimated from the saturation level and the clump sizes from K05.

Although there is significant estimation error in the DACF due to the limited sampling of the stochastic scintillation pattern, those masers with larger  $\mu$  also tend to show deeper first minima in the DACF. This is also consistent with the sources with lowest  $\mu$ , thought to be fully saturated, having  $\theta_S > \theta_F$ . Rickett et al. (2002) showed that anisotropic scattering in a thin screen produces a deep first minimum or “negative overshoot” in the ACF, and as the source becomes more extended, this “negative overshoot” is suppressed. A deep first minimum in the DACF is also seen for the intra-hour variable quasars and for the H<sub>2</sub>O masers in Circinus (McCallum et al. 2005), suggesting that anisotropic scattering in discrete “screens” is a widespread phenomenon.

There is some indication of nearby scattering along other lines-of-sight close to NGC 3079 from the MASIV VLA Survey (Lovell et al. 2003). The MASIV Survey found that, while a large fraction of all compact, flat-spectrum extragalactic sources vary with modulation indices typically in the range 0.01 to 0.1 at 5 GHz in a 72 hour period, only a tiny fraction (< 1%) have characteristic timescales of a few hours or less. J0949+5819, the closest MASIV source to NGC 3079 at an angular separation of 3.2°, showed variations with  $\mu = 0.15$  on a timescale of less than a few hours in 2002 January. This is likely to be due to scattering in a nearby screen within a few tens of pc. J0949+5819 was the most extreme variable observed in the first epoch of the MASIV Survey apart from the already known intra-hour variable J1819+3845 (Dennett-Thorpe & de Bruyn 2000). Of the nine MASIV sources within 10° of NGC 3079, five sources showed significant variability in at least three out of four observed epochs (Lovell et al., in preparation), namely J0949+5819, J0946+5020, J0929+5013, J0958+4725, and our calibration source J0958+655 which was also a previously known intra-day variable (IDV) (Wagner et al. 1993). While the fraction of nearby IDV sources is large but not exceptional, it is notable that the variations in J0929+5013 were also unusually rapid with a characteristic timescale less than a few hours. The presence of several rapid variables in the region of sky near NCG 3079 is suggestive of these sources being scattered by related structure in the very local Galactic interstellar medium.

The proposed scintillation model could be tested by measuring the time delays and correlation between the maser scintillation patterns arriving at two widely separated telescopes. Such a two-station time delay experiment, for example between the GBT and Effelsberg telescopes, should also allow a determination of the anisotropy in the scintillation pattern and its position angle as well

as the scintillation velocity (see e.g. Bignall et al. 2006).

It is worth noting that short timescale variability of masers can also be caused by gain variation along the maser amplification path. As the characteristic timescale of such variability is  $\sim L/c$ , where  $L$  is the maser length, for the H<sub>2</sub>O maser emission of NGC 3079 this implies a variability timescale of this type of  $\sim 10^5$  s. This is at least two orders of magnitude longer than the variability timescale detected here.

#### 4. SUMMARY

The full velocity range of the H<sub>2</sub>O megamasers in the accretion disk of NGC 3079 has been observed using the GBT in both RCP and LCP. This has enabled us to determine a sensitive  $1\sigma$  upper limit of  $\sim 11 \text{ mG}$  for the absolute poloidal magnetic field  $|B_\phi|$ . This corresponds to a  $3\sigma$  upper limit for the total magnetic field in the accretion disk of  $B_{\text{tot,lim}} = 40 \text{ mG}$  at  $\sim 0.64 \text{ pc}$  from the central black hole. This is the tightest magnetic field upper limit in an AGN accretion disk to date. The magnetic field upper limit corresponds to a mass accretion rate of  $\dot{M} \lesssim 10^{-1.7} M_\odot \text{yr}^{-1}$ , consistent with NGC 3079 accretion disk models and the X-ray luminosity.

In addition to the magnetic field measurements, the H<sub>2</sub>O maser lines of NGC 3079 were found to vary at characteristic timescales of the order of 1000 s. We conclude that this variability is due to weak scintillation caused by a scattering screen at  $\sim 25 \text{ pc}$ . The scintillation timescales and modulation index imply maser feature sizes of  $\sim 12 \mu\text{as}$  which corresponds to approximately 180 AU at the distance of NGC 3079. As the masers are found to be mostly saturated, maser beaming considerations imply that the masers occur in clumps with a size of  $\sim 0.002 \text{ pc}$ , consistent with the model for a thick, clumpy accretion disk.

This research was supported by a Marie Curie Intra-European fellowship within the 6th European Community Framework Program under contract number MEIF-CT-2005-010393.

#### REFERENCES

- Bignall, H. E., Jauncey, D. L., Lovell, J. E. J., Tzioumis, A. K., Kedziora-Chudczer, L., Macquart, J.-P., Tingay, S. J., Rayner, D. P. & Clay, R. W. 2003, ApJ, 585, 653
- Bignall, H. E., Macquart, J.-P., Jauncey, D. L., Lovell, J. E. J., Tzioumis, A. K., Kedziora-Chudczer, L. 2006, ApJin press, arXiv:astro-ph/0608619
- Blandford, R. D., & Payne, D. G. 1982, MNRAS, 199, 883
- Cordes, J. M., & Lazio, T. J. W. 2002, ArXiv Astrophysics e-prints, arXiv:astro-ph/0207156
- Dennett-Thorpe, J., & de Bruyn, A. G. 2000, ApJ, 529, L65
- Edelson, R. A., & Krolik, J. H. 1988, ApJ, 333, 646
- Elitzur, M. 1994, ApJ, 422, 751
- Fiebig, D. & Güsten, R. 1989, A&A, 214, 333
- Fiedler, R. L., Dennison, B., Johnston, K. J., & Hewish, A. 1987, Nature, 326, 675
- Fiedler, R., Pauls, T., Johnston, K. J., & Dennison, B. 1994, ApJ, 430, 595
- Greenhill, L. J., Ellingsen, S. P., Norris, R. P., Gough, R. G., Sinclair, M. W., Moran, J. M., & Mushotzky, R. 1997, ApJ, 474, L103
- Hawley, J. F., Gammie, C. F., & Balbus, S. A. 1996, ApJ, 464, 690
- Henkel, C., Guesten, R., Downes, D., Thum, C., Wilson, T. L., & Biermann, P. 1984, A&A, 141, L1
- Herrnstein, J. R., Moran, J. M., Greenhill, L. J., Blackman, E. G., & Diamond, P. J. 1998, ApJ, 508, 243

Humphreys, E. M. L., Greenhill, L. J., Reid, M. J., Beuther, H., Moran, J. M., Gurwell, M., Wilner, D. J., & Kondratko, P. T. 2005, *ApJ*, 634, L133

Irwin, J. A., & Saikia, D. J. 2003, *MNRAS*, 346, 977

Kondratko, P. T., Greenhill, L. J., & Moran, J. M. 2005, *ApJ*, 618, 618 (K05)

Lovell, J. E. J., Jauncey, D. L., Bignall, H. E., Kedziora-Chudczer, L., Macquart, J.-P., Rickett, B. J., & Tzioumis, A. K. 2003, *AJ*, 126, 1699

Maloney, P. 2002, *Publications of the Astronomical Society of Australia*, 19, 88

McCallum, J. N., Ellingsen, S. P., Jauncey, D. L., Lovell, J. E. J., & Greenhill, L. J. 2005, *AJ*, 129, 1231

Modjaz M., Moran J. M., Kondratko P. T., Greenhill L. J., 2005, *ApJ*, 626, 104 (M05)

Nedoluha, G. E. & Watson, W. D. 1992, *ApJ*, 384, 185

Neufeld, D. A., Maloney, P. R., & Conger, S. 1994, *ApJ*, 436, L127

Rickett, B. J., Kedziora-Chudczer, L., & Jauncey, D. L. 2002, *ApJ*, 581, 103

Sarma, A. P., Troland, T. H., Crutcher, R. M., & Roberts, D. A. 2002, *ApJ*, 580, 928

Sarma A. P., Troland T. H., Romney J. D., 2001, *ApJ*, 554, L217

Sawada-Satoh, S., Inoue, M., Shibata, K. M., Kameno, S., Migenes, V., Nakai, N., & Diamond, P. J. 2000, *PASJ*, 52, 421

Sofue, Y. 1999, *Advances in Space Research*, 23, 949

Trotter, A. S., Greenhill, L. J., Moran, J. M., Reid, M. J., Irwin, J. A., & Lo, K.-Y. 1998, *ApJ*, 495, 740

Vlemmings, W. H. T. 2006, *A&A*, 445, 1031

Vlemmings, W. H. T., Diamond, P. J., & van Langevelde, H. J. 2002, *A&A*, 394, 589

Vlemmings W. H. T., Diamond P. J., van Langevelde H. J., Torrelles J. M., 2006, *A&A*, 448, 597

Wagner, S. J., et al. 1993, *A&A*, 271, 344

Walker, M. A. 1998, *MNRAS*, 294, 307

Watson, W. D., & Wyld, H. W. 2000, *ApJ*, 530, 207

Yamauchi, A., Nakai, N., Sato, N., & Diamond, P. 2004, *PASJ*, 56, 605